

# Towards a Microfluidic Disease Detection Device Based on Cellular Adhesion Differences

by

Kristen M. Naegle

B.S. Electrical Engineering  
University of Washington, 2001

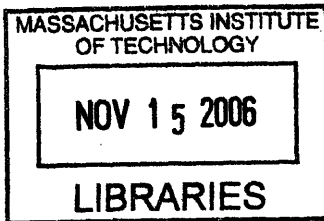
M.S. Electrical Engineering  
University of Washington, 2004

Submitted to the Department of Biological Engineering in Partial  
Fulfillment of the Requirements for the Degree of Master of Science in  
Biological Engineering

at the

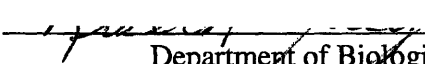
Massachusetts Institute of Technology

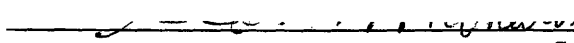
September 2006

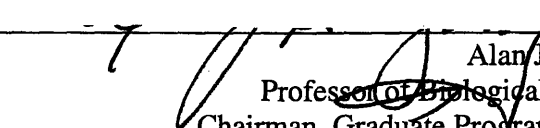


© 2006 Massachusetts Institute of Technology  
All rights reserved

**ARCHIVES**

Signature of Author   
Department of Biological Engineering  
May 19, 2006

Certified by   
Scott Manalis  
Associate Professor of Biological Engineering  
Thesis Supervisor

Accepted by   
Alan J. Grodzinsky  
Professor of Biological Engineering  
Chairman, Graduate Program Committee

# Towards a Microfluidic Disease Detection Device Based on Cellular Adhesion Differences

by

Kristen M. Naegle

Submitted to the Department of Biological Engineering on May 19, 2006 in Partial Fulfillment of the Requirements for the Degree of Master of Science in Biological Engineering

## **ABSTRACT**

There is a great need in the fields of biology, medicine, and pharmaceuticals to create high-throughput devices for the detection of specific cell states in a heterogeneous mixture of cells. The desire is to differentiate among diseased and healthy cells, cell age, and cell type with the minimum amount of sample pretreatment. This project addresses this need by developing microfluidic devices that exploit the adhesion differences between cell states and cell types to rapidly count cells of different types without the need for labels. There are two avenues in which to explore cell adhesion differences with these devices, the first is a net electrostatic change at the surface of the cell wall and the second is the presence of specific cell-membrane adhesion proteins. It is hypothesized that the forced interaction of the cell wall with the microfabricated microcapillary walls would result in a differential velocity based on cell type that could be detected simply using a microscope and video camera or an interferometer. The eventual integration of cell velocity detection would result in a portable all-inclusive lab-on-a-chip system that could be used in the field for detecting the presence of diseases, such as malaria and cancer as well as in a lab setting for drug discovery.

Thesis Supervisor: Scott Manalis

Title: Associate Professor of Biological Engineering

## **Acknowledgements**

The author would like to thank Dr. Scott Manalis for his thoughtful guidance and support as well as Dr. Subra Suresh for his generous help in the area of *Plasmodium falciparum*.

The author would also like to thank the following people for discussions and guidance during the course of this work: MTL Staff; Nanoscale Sensing Lab Members: Thomas Burg, Michel Godin, Johnson Hou, Andrew Sparks, and Philip Dextras; Suresh Research Group Members, John P. Mills, and Monica Diez.

## Table of Contents

ABSTRACT.....	2
Acknowledgements.....	3
Table of Contents.....	4
Introduction.....	5
Background.....	7
<i>Plasmodium Falciparum</i> .....	7
Current Methods of Diagnosing Malaria.....	8
Cell Staining – gold standard.....	8
Rapid Malaria Tests (RBT's).....	9
Device Motivation.....	10
Electrostatic Adhesion Differences PRBC.....	10
Electrophoresis.....	11
Specific Protein Adhesions.....	13
Previous work in Malaria Adhesion.....	14
Device Design and Fabrication.....	17
Silicon Processing.....	18
Pyrex Processing.....	20
Device Theory.....	22
Gate Capacitance.....	29
Cell-Wall Double-Layer Interactions.....	30
Device Testing.....	32
Device Verification.....	32
Measuring Cell Velocity.....	34
Video Microscopy.....	34
Interferometry.....	35
Streaming Currents.....	36
Testing Cell-Wall interactions.....	37
Adhesion Receptor Device.....	40
Surface Functionalization.....	40
Testing and Modeling.....	41
Conclusion.....	43
References.....	44
Table of Figures.....	46
Table of Equations.....	47
Appendix – Process Flow.....	48

## **Introduction**

The unique control of the same genome in a complex multicellular organism produces a wide range of cell types. These cell types are distinguished from each other based on their function in the body, but from an extracellular view, are differentiated based on subtle differences in protein production, secretory as well as membrane-bound, and mechanical response. The presence of a parasite, virus, or genetic disease enhances these differences further. In the case of a virus or parasite, additional genomic information has been introduced to the cell and therefore results in the production of foreign membrane and secretory proteins. Genetic diseases or cancer can result in the production of proteins that are normally “off” or the over- or under- production of normally “on” genes. These shifts in gene production can result in many phenotypic changes, including the increase or decrease of cellular adhesion and cell stiffness.

Some of these extracellular cues have been utilized in biological assays to detect the presence of disease. For example, detection of prostate specific antigen in human serum is used to diagnose the presence of prostate cancer. However, visual inspection of cell biopsies and blood is the most common technique used to detect the presence of most cancers and diseases. For example, staining and visual inspection of blood smears is the gold standard method of malaria diagnosis (Gascoyne P. et al. 2002), despite the fact that the most deadly form of malaria affects third-world countries in Africa that don't have the money or infrastructure to support widespread testing in this manner (WHO 2006). The need to improve testing availability, reliability and cost-effectiveness for disease diagnosis is the driving force for lab-on-a-chip diagnostics. The long-term vision for these systems is a stand-alone, disposable, and inexpensive devices that

can reliably diagnose the presence of disease at the point-of-care from a very small biological sample.

This project aimed to develop lab-on-a-chip technology that utilizes the naturally occurring extracellular clues of adhesion differences to detect the presence of diseased cells in a biological sample via a high-throughput method of cell counting. The immediate goal of this project is to develop a device for the detection of malaria given the acute need for such a device. However, the device could be applied to other diseases, like sickle cell anemia and cancer, and to other applications like distinguishing cell types, including the detection of stem cells, as well as monitoring the effect of drugs. Additionally, these devices could be used to explore basic biological adhesion interactions in a fluidic environment and in a high-throughput manner.

It is hypothesized that the device presented in this document will achieve the project aims by inducing a detectable cell velocity difference in a microcapillary based on adhesion properties, either general electrostatic changes in the diseased state, or the presence of specific adhesion proteins. The devices microfabricated in this project can be applied to both of the former cases, where utilizing it purely electrostatically would allow for the easy application of it to many different cell types and disease states. However, the device modeling and cellular interaction is unknown, making this a riskier option. This document will first discuss the background work that has been done leading to the development of this device with regards to both the electrostatic device and the adhesion protein device. Next, it will discuss the design requirements considered during fabrication and the fabrication steps. Finally, it will discuss specific device theory, modeling, and testing as applied to both devices individually.

## **Background**

### ***Plasmodium Falciparum***

One million of the 300 million cases of acute malaria are fatal, and 90% of these deaths occur in Africa, where the deadliest malaria parasite, *Plasmodium falciparum*, thrives (WHO 2006). Parasitized red blood cells (PRBC) go through a characteristic lifecycle following *P. falciparum* infection. In the first stage, ring stage, there is a visible lesion resulting from the invasion of the merozoite (Nagao E. 2000). Following the ring stage comes the early trophozoite state, late trophozoite stage, and finally schizont stage. The PRBC finally burst following schizont stage, releasing daughter merozoites, which go on to infect more red blood cells and again the cycle is repeated. In trophozoite and schizont stages, characteristic protrusions (knobs) form and increase in number with the advancement of infection (Gruenberg J. 1983; Nagao E. 2000), see Figure 1. These knobs are electron-dense and the site of membrane-bound adhesion proteins that are responsible for cytoadherence, which is believed to be the cause of severe clinical symptoms of malaria (Gruenberg J. 1983; Cooke B. M. 2000). The presence of these adhesion proteins results in an increased adherence of PRBC to other PRBC (autoagglutination), to healthy RBC (rosetting) and to endothelial cells. These adhesive interactions are believed to contribute to the blockage of microvasculature and therefore the high mortality rate of Falciparum malaria (Cooke B. M. 2000).

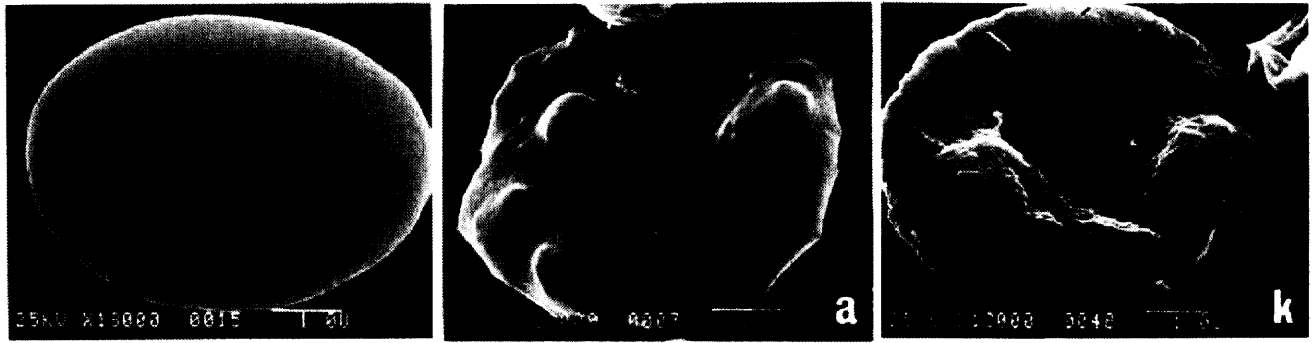


**Figure 1: Comparison of a healthy red blood cell, a red blood cell in trophozoite stage, and a red blood cell in schizont stage (from left to right). Protrusions density increases with stage of infection. SEM images taken from (Gruenberg J. 1983).**

## **Current Methods of Diagnosing Malaria**

### **Cell Staining – gold standard**

Cell smears and subsequent staining using Romanowsky stains are still considered the gold standard for detecting malaria in blood samples. According to (Kakkilaya 2006), an experienced technician can detect as few as 5 parasites/uL in a thick film, where thick films are prepared only for the detection of malaria. However, thin films are prepared in order to detect the type of malaria, in which case an experienced technician can only detect 200 parasites/uL, but can tell between the many forms of Plasmodium parasites. Staining is subject to inaccuracy due to mispractice of the staining technique, for example pH differences of the solution or waiting too long between sample collection and slide preparation. In addition to human error during preparation, cell staining could give a false response if there are too few PRBC circulating in the blood due to their sequestration in microvasculature or prior treatment with anti-malarial drugs (Kakkilaya 2006).



From thin smear stains, the percentage of infected red blood cells is determined by counting all the red blood cells on the slide and the number of infected cells. Finding the percentage of infected cells is important for ascertaining the severity of the infection. The speciation of infection is determined based on variations in the appearance of infected red blood cells when stained.

A second staining method that has been developed is the quantitative buffy coat test (QBC). This method involves the centrifugation of a blood sample in a cylindrical float and therefore separation of blood components based on densities. The red blood cell portion is then stained with an acridine orange stain, which is taken up by parasite DNA. The advantage of the QBC test over traditional cell smears is it takes only 15-30minutes to arrive at a result versus 60-120minutes (Kakkilaya 2006). However, the technique is a lot more costly due to the required materials and equipment. Smear tests only cost \$0.20-\$0.40 per test to perform (Kakkilaya 2006), but of course are limited to areas with the infrastructure to support such testing.

### **Rapid Malaria Tests (RBT's)**

Inexpensive testing methods for malaria that can be done in the field by inexperienced personnel are desirable considering the conditions where malaria persists. One avenue that has experienced growth in this area is in the detection of secreted proteins by the malarial parasite in the blood. These testing kits have achieved low cost, \$1.20-\$13.50 per test (Kakkilaya 2006) but have not yet been approved by the Food and Drug Administration for use in diagnosing malaria. This method of testing still faces many problems with incorrect results due to cross-reactions, difficulty reading the results by untrained individuals, and sensitivity. RBT's are currently much

less sensitive than microscope assays, 100 parasites/uL versus 5 parasites/uL for the smear studies. Also, RBT's are not capable of determining therapeutic effectiveness since antigens continue to circulate in the body even after effective treatment (Kakkilaya 2006).

## **Device Motivation**

### **Electrostatic Adhesion Differences PRBC**

The presence of the protein and electron dense knobs on the surface of PRBC means that there is possibly a net surface charge difference between healthy RBC and PRBC. Since the density of these protrusions increases with infection stage, it's possible that the surface charge also changes with infection stage. A microcapillary device was built, whose wall charge is controlled with a gate voltage applied to a conductor separated from the solution by an insulator, Figure 2a. The applied voltage,  $V_g$ , can control the sign and density of wall charge. The hypotheses to be tested is that complementary wall charges of the device and the parasitized red blood cells will oppose the fluidic forces and slow the PRBC. Healthy RBCs, that have a different wall charge, will be affected to a lesser extent and therefore can be differentiated from PRBCS based on their higher passage velocity. The channel dimensions of the device must be small enough to ensure direct interaction between the cell membrane and the capillary wall. Microfabrication is capable of making such channels (on the order of  $2\mu\text{m}$ ).

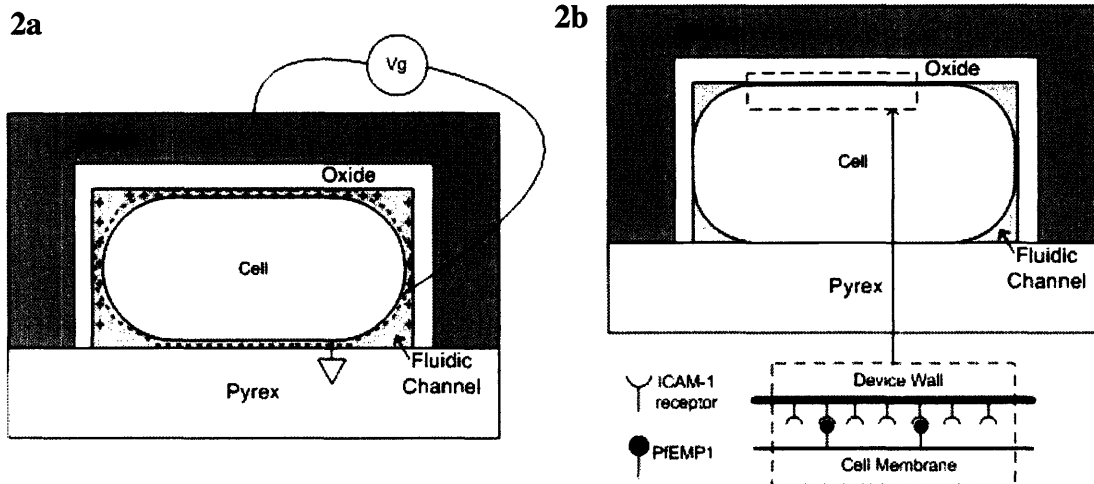


**Figure 2: a) Cross-section of proposed microfluidic FET device (not drawn to scale). Controllable wall charge of device allows for optimal interaction between device walls and cell wall of parasitically infected RBC. b) Picture of proposed microcapillary device, whose walls are functionalized with a receptor protein. Interactions between the cell membrane proteins and the wall receptors result in a velocity decrease of diseased cells.**

## Electrophoresis

Electrophoresis has long been used to explore the differences in the electrical characteristics of cell membranes. Over the years various modes of electrophoresis have been developed, for example free flow electrophoresis and capillary electrophoresis (Mehrishi J. N. et al. 2002) for both observation of electrical characteristics and separation of cell types based on differing electrophoretic mobilities (EPM). It is the information from these studies that indicates a device that utilizes cell surface charge for detection could be successful.

Cell electrophoresis suffers from a few serious drawbacks: electroosmotic flow, heating, electrolysis and long separation times. Electroosmotic flow is induced in the system when charged walls are present in the device, which is true for most experiments since untreated glass

capillaries are negatively charged at physiological pH. The two major avenues for treating electroosmotic flow in microcapillary experiments is to either measure the flow velocity due to EOF alone and remove it from the calculation of the EPM (Omasu F. et al. 2005) or to oppose EOF by neutralizing the wall charge (Ichiki T. et al. 2002). Heating and electrolysis are both a function of the large voltages required to perform electrophoresis. Electrolysis poses significant problems by creating bubbles and producing pH gradients in the channel (Minerick A. R. et al. 2002). The pH gradients not only produce variable electroosmotic flow patterns throughout the channel, but affect the electrophoretic mobility of the cell as well. Separation times for cells can be on the order of hours, which is not only undesirable from a convenience viewpoint, but also means temperature stabilization is required for cell viability. One solution for this is to only capture EPM data for a few cells (Slivinsky G. G. et al. 1997) which, reduces the statistical significance of the data, especially if the researcher is not aware of cell heterogeneity in the sample.

The wealth of information from electrophoresis experiments does indicate the possibility of using the proposed voltage controlled device for a number of different cellular applications. For example, human T-cells have an EPM that is more than 30% greater than B-cells (Slivinsky G. G. et al. 1997). For the case of diseased cells, malignant human epithelium cells have an EPM that is 13% greater than healthy epithelium cells (Slivinsky G. G. et al. 1997). Also, in pigmented hamster melanoma cells, it's been indicated that state of metastaticity is dependent on differential cellular EPM (Hyrce et al. 1993). The change in wall charge of *P. Falciparum* infected erythrocytes does not appear to have been studied previously.

## **Specific Protein Adhesions**

Although the surface charge of PRBC is unknown currently, the adhesion proteins responsible for cytoadhesion have been studied. The devices voltage controlled microcapillaries developed above can simply be used as microcapillaries for this implementation. In this second methodology, the capillary walls can be functionalized with adhesion receptors and their interaction with adhesion proteins on the cell will impede passage through the device, see Figure 2b. The application of pressure-driven flow will ideally prevent total cell arrest in the channel. Since the adhesion proteins are specific to the disease state of the cell, it is expected the velocity of healthy RBC will be unaffected and that the effect on velocity will increase with infection stage given the increase in knob density, and therefore, adhesion protein density. Figure 3 shows the proposed adhesive interactions that occur between PRBC and endothelial cells of the vasculature and other RBC (Cooke B. M. 2000). The PRBC image shows the parasite proteins, KAHRP and PfEMP3, which are responsible for knob formation as well as the surface proteins responsible for adhesion. The broken arrows indicate interactions that are not entirely proven, whereas unbroken arrows indicate those interactions that have been well supported (Cooke, 2000). Therefore, this project could utilize CSA, ICAM-1, HS, CD36, PECAM-1, or TSP as capture proteins on the wall surface. Since increases in adhesion of PRBC are indicated to be the cause of the severity of malaria infections, drugs developed to interrupt this adhesion process would greatly reduce the severity of the infection. Therefore, this device is ideal for not only detecting the presence of infected erythrocytes in a sample of blood, but also as a tool for monitoring the efficacy of drugs intended to interrupt adhesive interactions of PRBC, as well as potentially a high throughput method for testing adhesion-receptor interactions.

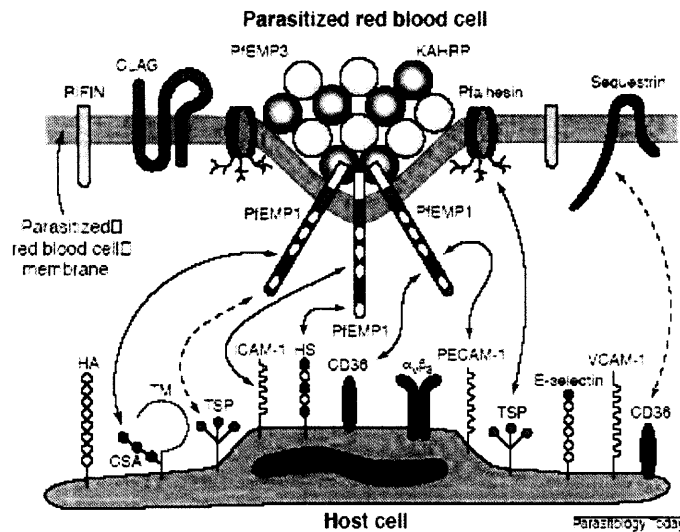


**Figure 3: Interactions occurring between a PRBC and an endothelial cell resulting from parasite encoded adhesion proteins (Cooke, 2000).**

### **Previous work in Malaria Adhesion**

What is now known about PRBC interactions with endothelial cells, healthy RBC cells, and PRBC was discovered using adhesion assays, both single cell and population assays. Some of the original discovery involved static adhesion testing where either target proteins, like CD36 and ICAM-1 were immobilized in Petri dishes, or cells expressing those proteins were immobilized on Petri dishes. PRBC were then introduced and after allowing time to settle, unadhered cells were washed out (Nash G. B. et al. 1992). Adhesion was then measured as a function of percentage that remained adhered. However, it was later found that when a similar test was performed under flow conditions, which more closely mimics the microvasculature environment, some adhesion relationships changed. For example, it was found that TSP, which has shown adhesion under static conditions, no longer adhered under the stress of flow (Cooke B.M. et al. 1995). Data suggests that CD36 and CSA interactions with PRBC have similar attachment characteristics that are resistant to flow disruption up to about 1 Pa of shear stress

(Cooke B. M. et al. 1996). However, interactions with ICAM-1 perform rolling-like behavior that's very similar to leukocyte rolling behavior (Nash G. B. et al. 1992). It was suggested by their behavior in flow assays, that ICAM-1 has a higher affinity for its target proteins than CD36, but CD36-PfEMP-1 interactions, once formed, were stronger under stress (Nash G. B. et al. 1992).

Single cell micropipette manipulation assays have also been performed to study the adhesion forces between PRBC and target cells (Nash G. B. et al. 1992). Although flow conditions suggested different adhesion forces between CD36 and ICAM-1, the pipette aspiration studies showed both required detachment forces on the order of  $10^{-10}$ N (Nash G. B. et al. 1992). However, quantification of single protein-protein interactions and the total number of interactions occurring between the two cells was not done for either the flow assays or the cell-cell pipette assays, making it difficult to make any true predictions of receptor-protein interaction strengths.

The main conclusion that was reached by the previous studies under flow is that flow conditions are necessary to observe the true behavior of PRBC in the vasculature system. However, parallel plate flow assays are only 1.5% efficient due to their large size (the smallest dimension is on the order of 100 $\mu$ m) (Cooke B.M. et al. 1995). Therefore, parallel plate flow assays are not ideal for high throughput cell counting of heterogeneous cell populations. This device could be used for both cell counting and high throughput adhesion characterization of cells and specific receptors. One final caveat to these results is that the cultured *P. falciparum* strains used in most adhesion

assays show different adhesion characteristics than their counterparts found in infected individuals (Cooke B. M. et al. 1998).



## Device Design and Fabrication

The following design requirements for the electrostatic microcapillary devices were met by microfabrication of pyrex and silicon wafers, which were then be anodically bonded forming a sealed fluidic channel. In order for the device wall charge to interact with the cell surface charge, the channels must be smaller than the cell diameters in at least one dimension. Of course, as the stage of *P. falciparum* infection advances, cell stiffness increases, and therefore passage of the cells through dimensions smaller than the cell may be impossible. However, (Shelby P.J. et al. 2003) showed that channel height of 2 $\mu\text{m}$  allowed passage of all cells, but not all channel widths did, Figure 4. Therefore, using (Shelby P.J. et al. 2003) as a design guide, widths of 2  $\mu\text{m}$ , 4  $\mu\text{m}$ , 8  $\mu\text{m}$ , 16  $\mu\text{m}$ , and 20  $\mu\text{m}$  were fabricated. The initial channel height is 2  $\mu\text{m}$ , but can be easily increased if necessary by modifying the channel etch time. Future testing may require varying channel height to observe the effect of mechanical stress on cell electrical properties. The channel length is somewhat arbitrary, 200  $\mu\text{m}$  would be sufficient considering that is the field of view through a high-power objective. However, in pressure-driven flow, the velocity is proportional to the partial differential of pressure with respect to length. Therefore, a lower velocity can be achieved with the same pressure applied by increasing the length. Two millimeters was chosen as the final channel length.

Of course, the major design requirement for the microcapillaries is a thin layer of oxide covering the gate electrode of the channel, thereby ensuring electrical isolation. There is a design tradeoff between gate capacitance, and therefore wall charge response, and oxide breakdown. An oxide thickness of 500nm was grown to meet the both of these requirements. The oxide breakdown will occur at 400V when the oxide is 500nm thick. All processing, unless otherwise noted, was

done either in the Microsystems Technology Laboratory, on MIT's campus, or in the Nanoscale Sensing Laboratory.

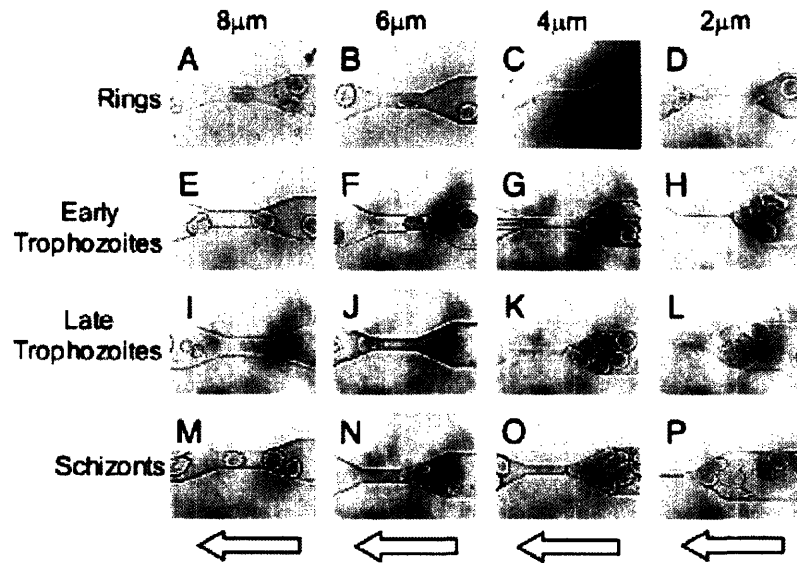


**Figure 4: (Shelby P.J. et al. 2003) Microcapillary constrictions 2µm high, with varying widths shows that later stages of PRBC cannot pass through channel widths smaller than 6µm. Arrow indicate direction of pressure driven flow.**

### Silicon Processing

Two major features must be etched into a double-side polished wafer. Both sides of the silicon wafer must be polished in order to ensure a good fluidic seal. Through-holes etched through the entire wafer will provide fluidic input into the channel. This can be done using a long 85degC, 25% w/v KOH etch. A sacrificial silicon nitride mask must first be grown. Since the nitride mask will act as an etch stop, the unpatterned side of the wafer will still have an intact nitride layer, which will allow for the patterning of the microcapillaries. Once the nitride membrane is patterned using a Reactive Ion Etcher (RIE), several methods can be employed to etch the actual fluidic channel in the silicon. Wall smoothness is paramount in order to reduce cell mechanical stress and ensure nonturbulent flow. Therefore, both wet and dry etches were performed for

comparison. Using the same conditions as the through-hole KOH etch produced very rough channels. However, using a  $CF_4$  based dry etch appeared to produce very smooth channels and so this method was employed for final device production.

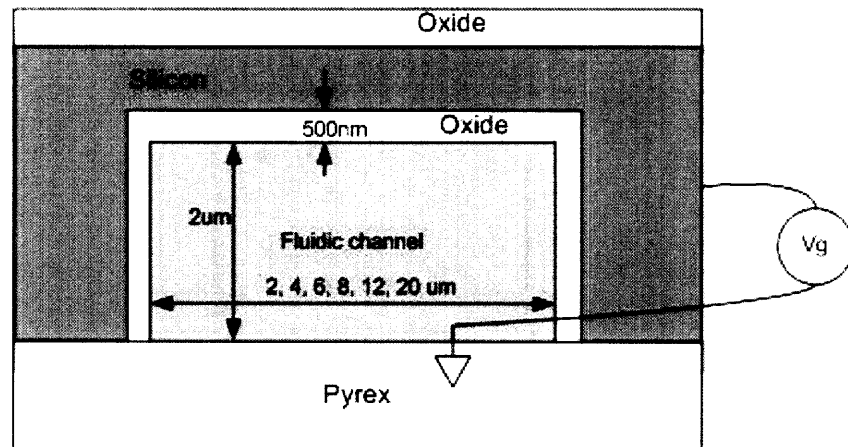


**Figure 5: Cross section of proposed device (not drawn to scale). Initial channel height, 2µm. Device widths ranging from 2-20µm.**

Once both the through-holes and the microchannels are etched in the silicon, the sacrificial nitride membrane must be removed, using a hot phosphoric acid bath. Nitride could be used as the insulator in the voltage controlled microcapillary, however the properties and surface chemistry of silicon dioxide are better understood. Therefore, the final step in the silicon process, prior to bonding with the pyrex wafer, is to thermally grow the oxide insulator, ensuring electrical isolation in both the through-holes and the channel area. Silicon will provide the electrical gate contact, and will cover the entire channel. Later device designs can use metal traces allowing wall control over very specific parts of the channel. As shown in Figure 5, once the individual devices are die-sawed from the wafer, an electrical contact to the silicon can be made from the side. An Ag/AgCl wire in one of the fluid ports will provide a ground reference.

It was found during processing, that the KOH etch made the devices extremely fragile during further processing steps, and many wafers were lost during additional wet steps such as the hot phosphoric bath and also piranha cleaning steps. In future processing, it might be desirable to first dry etch the microchannels in the silicon wafer, and then grow the nitride mask for the KOH through-hole etch. This will move most processing steps to occur before the wafer's strength is compromised by the KOH etch.

### **Pyrex Processing**

Anodically bonding the channel side of the silicon wafer to pyrex will ensure an enclosed fluidic channel and allow an optical window into the channel. There are two options, 1) Bond the silicon to an unprocessed glass wafer, where the silicon channels are directly connected to the through holes 2) Etch large bypass channels into the glass which connect the through-holes to the silicon channels. The advantage of the second method is lower pressures are required to fill the channel. Although the anodic bond will certainly withstand these pressures, the o-rings and external tubing manifold may not. The disadvantage of using bypass channels is a minimum pressure is required (Thomas Burg 2006) to induce cell movement from the bypass channel into the microchannel. This required pressure differential, upon first testing, produces cell speeds that are too fast to optically determine with a low frame-rate camera. All of these potential problems will need to be addressed in the testing stage of the devices, i.e. pressure requirements, manifold constraints, and minimum flow velocity. The latter problem could be addressed by the purchase of a high frame-rate camera or using a different velocity measurement method.

For the pyrex processing in the case of bypass channels, an amorphous silicon mask can be patterned and hydrofluoric acid can be used to isotropically etch the Pyrex bypass channels. This method has been proven previously in the Nanoscale Sensing Lab to produce a smooth 2:1 etch. The silicon mask works best if deposited using LPCVD (low pressure chemical vapor deposition), which is done at the University of California Berkeley facilities. An anodic bonding process was used to permanently bond the silicon and pyrex wafers.



**Figure 6: Microscope pictures of fabricated devices a) 8 $\mu$ m snake-like channel and bypass on left b) Glass bypass and silicon through-hole interconnect**

## Device Theory

The success of the electrostatic device is dependent on the ability to control the device wall charge. Therefore, this section will explore the wall charge dependence on the applied gate voltage as a function of physical constraints in the system. First, the double layer model as a function of intrinsic wall charge will be developed. Next, an extension of the double layer model will be introduced as a function of an applied gate potential. Finally, the effect of pH and intrinsic charge on device sensitivity will be explored. Traditional double-layer theory was employed in deriving this model, but especially with the guidance of notes provided by Jay T. Groves (Groves 1996). Only three of the four channel walls can be controlled in the manner presented since the fourth wall must be transparent for measuring cellular velocity. Also, double layer interactions occurring at the corners of the device has been neglected since at physiologic pH the debye length is much smaller than the channel widths.

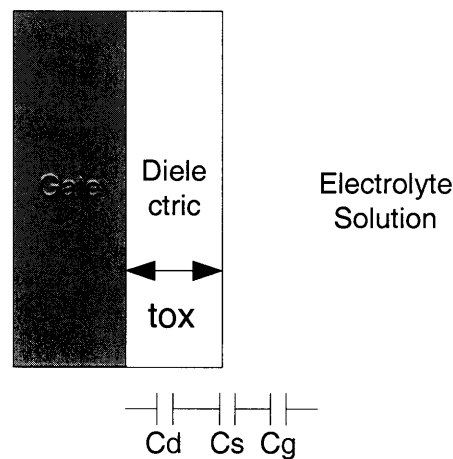


**Figure 7: Depiction of dielectric-solution interface with metal electrode gate. The double layer, consisting of the compact Stern layer (Cs) and the diffusion layer (Cg) are in series with the dielectric capacitance (Cd).**

For a normal double layer, the intrinsic potential across the double layer due to surface wall charge density  $\sigma$  can be described by the Gouy-Chapman equation

$$\text{Equation 1: Gouy Equation } \zeta_o(\sigma) = \left( \frac{2kT}{ze} \right) \sinh^{-1} \left( \frac{\sigma ze L_D}{2kT\epsilon} \right)$$

Where  $k$  is the boltzmann constant,  $T$  is temperature,  $z$  is valency of ionic buffer,  $e$  is the charge of an electron, and  $L_D$  is the debye length and is defined as:

$$\text{Equation 2: Debye length } L_D \equiv \left( \frac{kT\epsilon}{2Iz^2e^2} \right)^{\frac{1}{2}}$$

Where  $I$  is the concentration of the ionic solution and  $\epsilon$  is the dielectric constant of the solution, in this case water. The double layer can be modeled as two capacitors in series, the compact layer capacitance as described by Stern, and the diffuse layer capacitance, which can be found from the Gouy equation:

$$\text{Equation 3: Gouy Capacitance of the diffuse layer } C_G = \frac{\epsilon}{L_D} \cosh \left( \frac{ze\zeta}{2kT} \right)$$

Now, in order to take into account the applied potential, one can model the system as a series of three capacitances, Figure 7, the capacitor due to the dielectric insulator  $C_D$  (silicon dioxide in this case), Equation 4, the compact layer capacitance  $C_S$  and the diffuse layer capacitance  $C_G$ . The total capacitance is series combination of all three, however since  $C_D \ll C_G \ll C_S$ , the total capacitance is roughly equivalent to the capacitance across the dielectric,  $C_D$ . Viewing the system as a simple capacitive divider, the diffuse layer potential can be related to the applied voltage according to Equation 5.

$$\text{Equation 4: Capacitance due to the silicon oxide dielectric } C_D = \frac{\epsilon_{ox}}{t_{ox}}$$

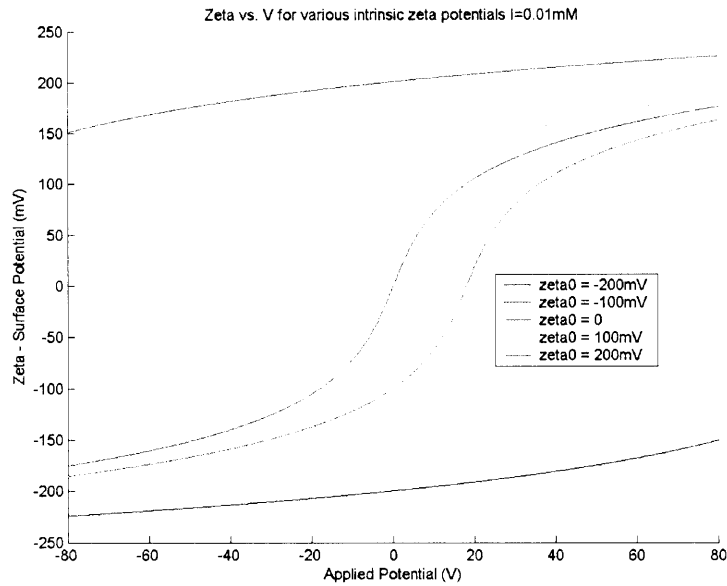
**Equation 5: Capacitor divider**  $dV = \frac{C_G}{C_D} d\zeta$

Integrating both sides and solving for  $\zeta$  results in a relationship that gives the new wall potential as a function of the intrinsic wall potential and the applied gate potential:

**Equation 6: Zeta potential with applied gate bias**  $\zeta(V) = \frac{2kT}{ze} \sinh^{-1} \left[ \left( \frac{zeL_D C_D}{2kT\epsilon} \right) V + \sinh \left( \frac{ze\zeta_o}{2kT} \right) \right]$

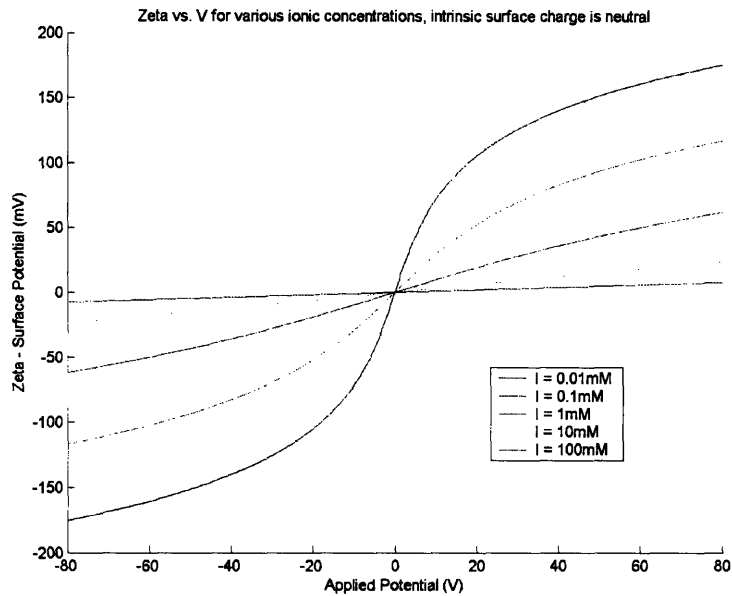
It's interesting to then study the effect of pH and salt concentration on the sensitivity of the device. The wall charge density, and therefore the intrinsic zeta potential, is a function of pH. Silicon dioxide at physiologic pH it is highly negatively charged since the surface is deprotonated. From Figure 8, one can see that the effect of intrinsic surface charge is to 1) compress the range over which the surface potential can be changed and 2) to shift the bias potential at which the surface is sensitive to a change. However, at extreme surface potentials, +/-200mV, one can see that the surface can no longer be appreciably altered given a large applied voltage.





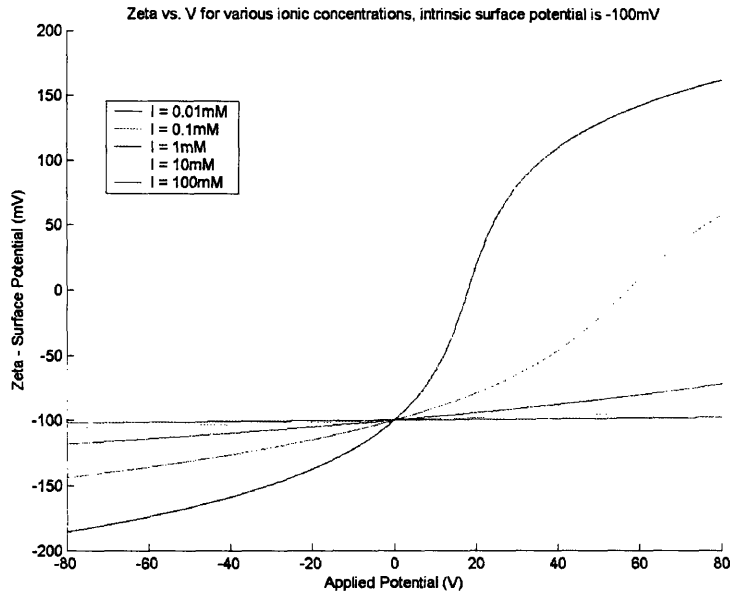
**Figure 8: Surface Potential vs. applied voltage as a function of intrinsic surface potential (which is dependent on solution pH).**

Figure 8 was modeled with an ionic concentration of 0.01mM. However, the ionic concentration has a direct impact on the debye length and therefore also an impact on the sensitivity of the device. Figure 9 shows the relation between the swing in zeta potential as a function of ionic concentration. This figure was derived assuming a neutral wall charge and therefore the swing is antisymmetric about zero volts. The increase in ionic concentration, and therefore the decrease in the debye length, acts to compress the range of achievable surface potentials. Physiologic ionic concentration for human cells is on the order of 150mM, which implies only a very small range of voltages can be developed at the surface.



**Figure 9: Zeta potential as a function of voltage for various ionic concentrations, and therefore debye lengths, with a neutral intrinsic wall charge.**

Finally, in Figure 10, both ionic concentration and a non-neutral wall charge of  $-100\text{mV}$  is considered. This figure clearly shows the need to neutralize the intrinsic wall charge when high ionic concentrations are required, since the ability to reverse the wall charge disappears at concentrations greater than  $1\text{mM}$ . Wall charge can be neutralized, of course, by using a solution with pH very near the wall's pKa. However, in the case of glass and silicon nitride, this is well below the required pH required for physiologic systems. Therefore, surface alteration using chemical functionalization will be required to neutralize the wall charge.



**Figure 10: Surface potential vs. voltage for varying ionic concentrations where intrinsic wall potential is -100mV.**

Wall neutralization is a key concern in electrophoresis as well, since electrophoretic mobilities must be separated accurately from any electroosmotic flow. One group looked at various glass coatings that could suppress EOF at physiologic pH and salt conditions. Omasu et. al. looked at three typical coatings that could be used to prevent nonspecific cell adhesion in microcapillary electrophoresis, bovine serum albumin (BSA), gelatin, and 2-methacryloyloxyethylphosphorylcholine (MPC). Their EOF results are shown in Figure 11. MPC appears to have zero charge at physiologic pH of 7.4, making it an ideal coating for this device. The method followed by (Omasu F. et al. 2005) to coat the channels was a 30minute dehydration directly preceding functionalization with MPC by filling and emptying the channel.

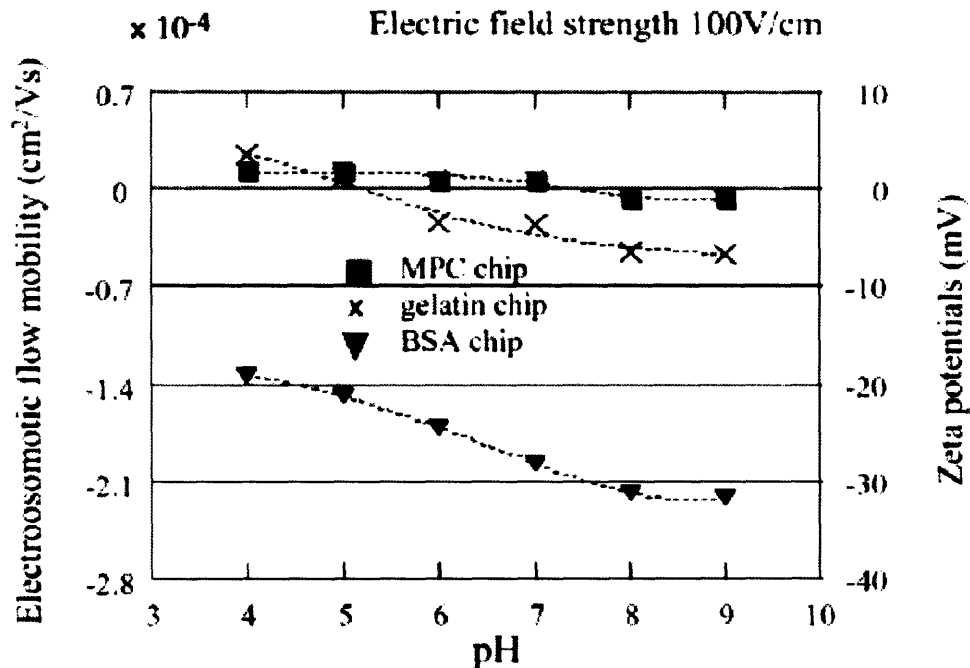


Figure 11: (Omasu F. et al. 2005) Comparison of different wall coatings and their effect on electroosmotic flow

N-cetyl-N,N,N-trimethyl ammonium bromide (CTAB) was used by Schasfoort et. al. to reduce the wall charge at physiologic pH (Schasfoort R. B. M. et al. 1999). This was not a channel pretreatment, but CTAB was simply added to the buffer. It reduces the wall charge, but does not completely neutralize it at pH 7.4. Another method used to significantly reduce electroosmotic flow in electrophoresis experiments is adsorption of Poly-N-hydroxyethylacrylamide (PHEA) (Methal N. Albarghouthi 2003). This method involves washing the capillary first with HCl to maximize protonation of the surface silanol groups and then adsorbing PHEA by washing with PHEA for 15minutes. Although this method does not completely eliminate EOF, it is a very stable protocol for significantly reducing EOF.

## Gate Capacitance

Initially it appears that the oxide thickness is a tradeoff between device sensitivity and breakdown voltage. However, as the oxide thickness is decreased, the required voltage to achieve a desired zeta potential will also decrease. It is desirable to quantify this tradeoff so that the optimum thickness can be chosen. Figure 12 demonstrates the relationship between the required gate voltage and the breakdown voltage for various oxide thicknesses between 100nm and 2 $\mu$ m thick. The required gate voltage was determined by Equation 7, where the desired zeta potential was 100mV. The breakdown voltage of silicon dioxide was assumed to be 8MV/cm. The intrinsic zeta potential was assumed to be -50mV, which mimics the case where PHEA was used to reduce wall charge, but has not eliminated entirely. In this case one can see that oxide breakdown will not actually limit the achievable zeta potential, but instead it will be limited by the high voltage supply.

**Equation 7: Voltage required to achieve a desired zeta potential**

$$V = \left( \frac{2kT\epsilon}{zeL_D C_D} \right) \left[ \sinh\left( \frac{ze\zeta}{2kT} \right) - \sinh\left( \frac{ze\zeta_o}{2kT} \right) \right]$$

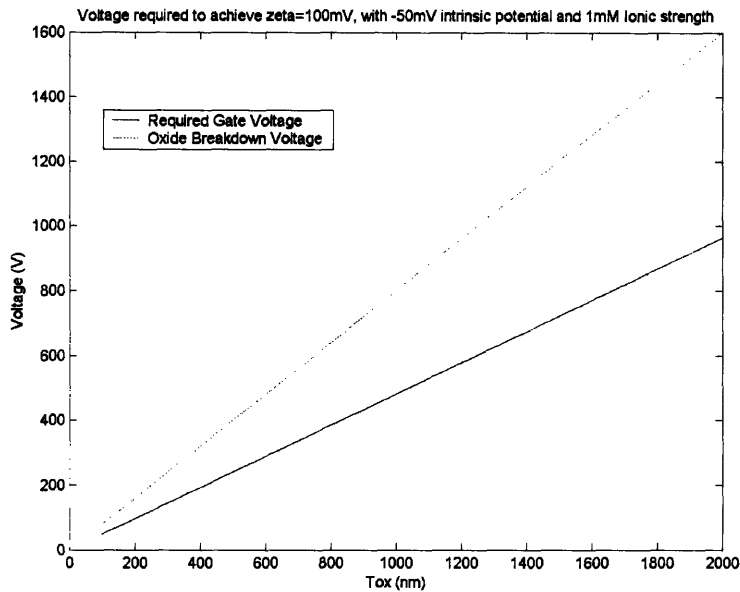


**Figure 12: Oxide breakdown voltage and gate voltage as function of oxide thickness. Gate voltage solved to achieve 100mV zeta potential with a -50mV intrinsic potential at 1mM ionic strength.**

### Cell-Wall Double-Layer Interactions

The effective wall charge for the device was derived previously as a function of ionic strength, intrinsic wall charge, and applied gate voltage, Equation 6. Ideally, the cell-wall interaction will result from cell-wall attraction based on opposite surface charges. However, there are many possibilities, seen and unforeseen, that could prevent the desired velocity effect from taking place. The problem of two charged surfaces interacting in an ionic solution is a complicated one. Even more so when one of those is a flexible cell wall made of a fluid phospholipid bilayer.

The interaction of oppositely charged double layers is prevented when the double layers are further than a debye length apart due to charge screening by the ionic solution. At high ionic strengths, the screening distance is very small, on the order of 1-10nm and therefore the channel

height of the device was made much smaller than the dimension of the cell in order to ensure an interaction between the cell wall and the device wall. However, will this system then cause particle exclusion between the cell wall and the device wall? In this case, the local pH and ionic strengths are indeterminable and therefore so are the effective wall charges of the two surfaces.

There was an observed phenomenon previously that when positively charged lipid bilayers were exposed to negatively charged particles, it induced a region in the bilayer that could bind to the oppositely charged particles, and a region that repelled the charged particles (Aranda-Espinoza H. et al. 1999). It was concluded that lipid mixing was responsible for space charge separation across the membrane. Clearly, this phenomenon could potentially exist in the interactions between the cell and the device complicating the predictive modeling and potentially limiting the sensitivity of the device.

## **Device Testing**

Testing of the electrostatic device falls into two major categories, first the verification of the device using electroosmotic flow (EOF) and second the verification that the wall charge can differentially interact with charged cell membranes affecting their passage velocity. In verifying the device, using EOF, the major outcomes should be to determine whether intrinsic wall charge at desired pH and ionic strengths can be neutralized and if the effective wall charge as a function of voltage is modeled correctly.

## **Device Verification**

One of the most common ways to measure EOF is to use a neutral flow marker, which can be monitored microscopically. It's necessary that the marker used is completely neutral so that its velocity represents only the fluid velocity and not an additional electrophoretic force. Any neutral marker can be combined with microscope analysis to measure particle velocity. However, a commercial particle image velocimeter (PIV) could also be used to measure EOF in the channel.

One of the first challenges in this project is neutralizing the intrinsic wall charge of the device. The necessity of this was described in the Device Theory section, where it was shown that at physiologic pH and ionic strength, the wall charge cannot be reversed given native charge groups of silicon dioxide. Proof that the employed surface chemistry neutralizes the wall charge can be accomplished by achieving zero EOF for any given applied voltage. Once this is proven, then EOF can be measured versus applied gate potential to verify the modeling and voltage-surface charge relationship. The fluid velocity due to an electroosmotic force is shown in Equation 8,



where  $E$  is the applied lateral electric field,  $\eta$  is the viscosity of the fluid,  $\epsilon$  is the permittivity, and  $\zeta$  is the modified wall potential.

$$\text{Equation 8: Fluid velocity resulting from electroosmosis } v_f = \frac{\epsilon}{\eta} \zeta E$$

Combining Equation 8 and Equation 6 results in the fluid velocity as a function of applied voltage, where  $\sigma_0$  is considered to be zero since intrinsic neutrality was proved during earlier testing. An example of the voltage dependency is shown in Figure 13. Since  $\sinh^{-1}(x)$  for  $x < 1$  approximately equal to  $x$ , then the electroosmotic flow velocity is roughly linearly dependent on both applied gate voltage and lateral electric field.

$$\text{Equation 9: Fluid velocity as a function of applied gate voltage } v_f = \frac{2kT}{ze} \sinh^{-1} \left[ \left( \frac{zeL_D C_D}{2kT\epsilon} \right) V \right] \frac{\epsilon}{\eta} E$$

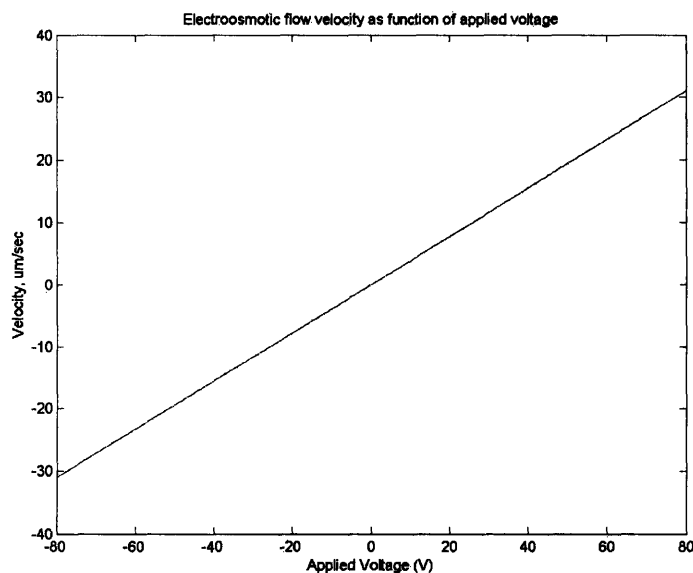


**Figure 13: Fluid velocity ( $\mu\text{m/s}$ ) vs. applied gate voltage for a  $50\text{V/cm}$  lateral electric field, zero intrinsic wall charge, and a  $100\text{mM}$  ionic strength solution.**

## **Measuring Cell Velocity**

Perhaps one of the most challenging aspects to this project is accurately measuring the velocity of a cell in the channel. One major setback to the implementation of the electrostatic device is that the difference in velocity between cell types of interest based on charge-charge interactions will be very small, and therefore a sensitive velocity measurement will be imperative. Luckily, many methods of measuring the velocity can be attempted, several of which take advantage of the transparency of the pyrex side of the channel.

## **Video Microscopy**

Video microscopy is perhaps the most straight-forward way of determining cell velocity in the microchannel. Simply implemented, a continuous camera image will be subject to particle tracking software, which will identify cell boundaries in the channel and monitor progression of the cell through the channel. A major disadvantage of this implementation is the frame rate of the camera will limit the speed that can be captured, and it's possible that the pressure driven flow required to force cells from the bypass channels into the microcapillary will result in flow velocity that is too fast for most reasonably priced cameras. Also, the reflectivity of the smooth silicon channels may obscure the cell boundaries. However, using monochromatic light at 400nm, where hemaglobin selectively absorbs (Sutton N. et al. 1997), will improve contrast between the cell and channel walls. A major advantage videomicroscopy is that cell volume can also be estimated using this technique. Dispersion in velocity measurements are predicted due to cell volume and surface area variations between cells. Normalizing each cell by its measured volume could reduce this data spread.



**Figure 14: Picture of straight 4 $\mu$ m channel. Boxes above and below channel designed to aid in image recognition.**

The fabrication masks for the microchannels were designed with videomicroscopy in mind. First, marks were added above and below the channels to aid in image recognition. Figure 14 shows a 4 $\mu$ m straight channel, which has a large box on top of the channel to mark the center, and smaller boxes below the channel to mark 50 $\mu$ m separations. Also, Figure 6a, shows the snake-like channels that were fabricated to increase the distance over which a cell will pass in a single microscope objective area, thereby accumulating a larger passage time.

### **Interferometry**

An interferometer utilizes the interference of a reflected beam to measure the distance between two reflecting plates. The reflection is of course also a function of the material between the two plates. Therefore, if a laser beam was directed at the back wall of the channel and its reflection detected by a photodiode, the change in optical density due to the presence of a cell in the channel would effectively modulate the reflected signal at the photodiode. Therefore, two beams could be used at two spots in the channel in order to detect the passage of a cell through the channel. The advantage of this system, particularly over videomicroscopy, is the signal conditioning becomes entirely electronic in nature. The signal will be converted from light to

current via a photodiode and the limitation in change in detectable transit time will essentially be determined by the spatial separation of the two beams in the channel.

### Streaming Currents

Electroosmotic flow is induced by an applied tangential electric field, Equation 8. The corollary to this is the streaming potential, which is the induction of a tangential field by an applied pressure gradient. Starting from the same basic equation, one can find the tangential field produced by the pressure driven flow by relating fluid velocity to the pressure gradient. It is assumed that in the absence of cells in the channel, fully developed poiseuille flow exists, since the channel is much longer than the entry length predicted by the low Reynolds number. Assuming one-dimensional flow for the rectangular channel, the average velocity can be related to the pressure drop across the channel by Equation 10, where  $\eta$  is the fluid viscosity,  $h$  is the channel height and the gradient of pressure is taken with respect to the tangential direction,  $x$ .

$$\text{Equation 10: Average fluid velocity for one-dimensional laminar flow } v_f = \frac{h^2}{2\eta} \frac{\Delta P}{\Delta x}$$

Plugging Equation 10 into Equation 8 and solving for the electric field, produces the result in Equation 11. Since the electric field can be related to the gradient of a voltage, one can see that the voltage drop across the capillary induced by pressure driven flow is directly proportional to the pressure gradient and inversely proportional to the zeta potential of the wall.

$$\text{Equation 11: Induced electric field due to streaming potential } E = \frac{\Delta V}{\Delta x} = \frac{h^2}{2\epsilon \zeta} \frac{\Delta P}{\Delta x}$$

When a cell enters the channel, it will disrupt the streaming potential since the cell size is on the same order as the channel. Therefore a cell entering the channel will change the measured voltage drop across the channel. Therefore, one way to monitor cell passage time is to measure the streaming potential changes with time. However, it is possible that the potential across the

channel will reflect only two states of the channel, a fluid filled channel with no cells and a channel with one or more cells.

### **Testing Cell-Wall interactions**

Following verification of the gate-charge relationship, it will then be time to test whether the wall-cell interaction will produce the desired effect on velocity. The effect can be simply shown using a healthy RBC and three wall charges, neutral ( $V=0$ ), positive wall charge ( $V=80V$ ), and a negative wall charge ( $V=-80V$ ). The cell velocity is expected to be maximally affected when the wall of the device is positively charged. There are several possibilities why at this point in the testing process a velocity difference cannot be detected as a function of gate voltage. The first could be measurement sensitivity as discussed in the previous section as a limit of the different measurement methodologies. The second reason could simply be that the electrostatic effect cannot significantly counteract the force in the lateral direction due to the pressure driven flow. Or finally, the wall charge of the device takes on an unpredictable value when the cell wall is introduced.

Ideally, a measurable velocity change is detectable as the gate potential is changed. The next step is to see if cellular wall charge densities can be differentially affected by the device wall charge. One way to do this is to artificially change the wall charge of a cell so that between cell types all other variables are identical and a change in velocity can be assumed to be produced only by the electrostatic interactions between the cells and the device. One model system for this is to artificially change the wall charge of erythrocytes by covalently binding polyethylene glycol (PEG) to the cell surface. Sabolovic et. al. performed PEG attachment to red blood cells using a

simple incubation step. They found the electrophoretic mobility changed by 15% (Sabolovic D. et al. 2000).

The electrophoretic mobility (EPM) is simply the velocity experienced by a particle divided by the forcing field. Much work has been done to model the forces acting on the particle in order to extract correctly the surface charge density from the EPM. One of the simplest models, which neglects surface conductivity and assumes a uniform surface charge is shown in Equation 12. The Huckel correction to Smulochowski's original relationship takes into account nonuniformities in the electric field surrounding a spherical particle (Camp J. P. et al. 2005). Using the Guoy-Chapman relationship, EPM can directly be related to surface charge density, Equation 13. Therefore, since testing conditions between RBC and PEG coated RBC remained the same, the 15% change in EPM is ideally a direct reflection of a 15% decrease in surface charge. Of course, the change in surface charge is potentially different then that reflected by the change in EPM due to surface charge density variations and other deviations from the model.

**Equation 12: Smoluchowski equation, with Huckel's correction, relating zeta potential and EPM**

$$EPM = \frac{U}{Eo} = \frac{2}{3} \frac{\epsilon \zeta}{\eta}$$

**Equation 13: EPM as a function of surface charge density**  $EPM = \frac{2}{3} \frac{\sigma}{L_d \eta}$

At this point in the testing stage velocity as a function of voltage for a RBC of known surface charge density has been recorded. Additionally, velocities for two cell types of different surface charge densities and various gate voltages have also been recorded. It is now ideally possible to develop a physically motivated model to relate cell passage velocity as a function of surface charge and gate voltage. Given an accurate predictive model, the sensitivity of the device to

surface charge densities can be determined based on the minimum detectable velocity change. Finally, the device is ready to be applied to a model system to detect cell types based on their unique surface charge densities, such as PRBC vs. RBC.

## **Adhesion Receptor Device**

The adhesion receptor device, Equation 2b, will produce a differential velocity between cell types by utilizing receptor-protein adhesions unique to one of the cell types. This implementation of the microcapillary device presents much less risk than that of the electrostatic device since flow based assays have already shown the possibility of inducing specific velocity changes. However, it cannot be extended to other cell populations easily and will require much stricter handling conditions in the field due to the receptor proteins that will either be covalently bound or physioabsorbed to the surface. Also, it will likely only be able to detect those cells, which are later in the parasite life cycle and have a large concentration of cell surface proteins. This limitation is worsened because those cells have been shown to sequester in the microvasculature of the body due to their increased adhesion, which means few of these cell types can be captured using a blood draw from the extremities. However, it does have the advantage of more accurately representing in vivo physiology and could therefore be used to observe therapeutic effects or perform high-throughput adhesion-receptor force interactions.

## **Surface Functionalization**

There are two surface functionalization techniques that could be used in this device. The first would be to culture cells, which present the desired receptors on their surface, for example human umbilical vein endothelial cells (HUVEC) which present ICAM-1 or the human amelanotic melanoma cell line (C32), which present both ICAM-1 and CD36 (Nash G. B. et al. 1992). The second method would be to functionalize the surface with just the proteins alone. This method has the advantage of eliminating interaction complexity. In the case of using



receptor-presenting cells, the device fabrication must be altered to allow for a single layer of cells on all four sides of the device.

Protocol for functionalizing a glass surface with CD36 or CSA involves first washing with nitric acid and then coating with poly-L-lysine, then incubating overnight at 4°C with either CD36 or chondroitin sulfate A (CSA) and then finally blocking with BSA (Cooke B. M. et al. 1998). Another paper by the same author (Cooke B. M. et al. 1993) presents a way of culturing protein-presenting cells on capillary walls. Prior to seeding the capillaries with HUVEC cells, a coating agent like gelatin or 3-aminopropyltriethoxy-silane (APES) was required to ensure cell growth. Cultured HUVEC cells were then added to the microcapillaries and allowed to attach and grow. The drawback to this functionalization method is the culture medium must be continually exchanged to ensure a constant pH due to the metabolization of the cells, temperature must be controlled, and sterilization is of the utmost importance to ensure cell viability.

### **Testing and Modeling**

Ideally, as with the electrostatic device, a predictive model can be developed to relate cell velocity as a function of the number of protein receptors on the cell and pressure gradient. As *P. falciparum* matures in a PRBC, the density of protein rich knobs will increase, and therefore the infection stage could also be detected. This predictive model will require knowing the density of proteins on the surface of the capillary walls, the forces applied by the pressure driven flow, and the contact area of the cell and device walls. The most important aspect of this device is specificity of interaction with diseased cells alone.

Assuming cell dimensions where the cell fills the entire channel, then pressure driven flow can apply a force on the cell on the order of 0.1pN to 20pN. According to the pipette aspiration experiments with ICAM-1 and CD36 one pN of force is required to pull a PRBC and a HUVEC cell apart (Nash G. B. et al. 1992) and therefore these flow rates should be enough force to prevent complete cell arrest . However, in this case, there are potentially many more protein-receptor interactions and therefore not enough force to prevent cell arrest. This requirement may aid in the choice of specific adhesion receptor used. For example, ICAM-1 interactions produce a rolling-like behavior in a flow cell, because although they have a high affinity for PfEMP-1, their interaction does not hold up under flow conditions like CD36-PfEMP-1 interactions. However, if ICAM-1-PRBC interactions are not sufficient to produce a measurable velocity change then CD36 or a combination of ICAM-1 and CD36 could be used.

## **Conclusion**

This document has explored the possible implementations of microfabricated microcapillary devices made for the use of high-throughput discrimination of cells. Utilizing the natural changes of cellular adhesion or surface charge differences between cell types and states could lead to a labelless detection system. This has great potential for many uses, including biological discovery and pharmaceutical testing. However, it's greatest potential lies possibly in the creation of a portable lab-on-a-chip device for disease detection in places where standard equipment cannot normally be used.

The two modes of adhesion based cell velocity differentiation were discussed. In conclusion, the electrostatic device has the advantage of requiring absolutely no surface chemistry making it immediately applicable to differentiating between any cell types, which have different surface charge densities. However, predicting the two double layer interactions was shown to be problematic and therefore the use of specific adhesion receptors was also introduced and may prove to be a guaranteed way to induce a velocity dependence that is highly specific to the disease state.

## References

- Aranda-Espinoza H., Chen Y., Dan N., Lubensky T. C., Nelson P., Ramos L. and Weitz D. A. (1999). "Electrostatic repulsion of positively charged vesicles and negatively charged objects." Science **285**: 394-397.
- Camp J. P. and Capitano A. T. (2005). "Size-dependent mobile surface charge model of cell electrophoresis." Biophysical Chemistry **113**: 115-122.
- Cooke B. M., Nicoll C. L., Baruch D. I. and Coppel R. L. (1998). "A recombinant peptide based on PfEMP-1 blocks and reverses adhesion of malaria-infected red blood cells to CD36 under flow. ." Molecular Microbiology **30**(1): 83-90.
- Cooke B. M., Rogerson S. J., Brown G. V. and Coppel R. L. (1996). "Adhesion of malaria-infected red blood cells to chondroitin sulfate A under flow conditions." Blood **10**: 4040-4044.
- Cooke B. M., Usami S., Perry I. and Nash G. B. (1993). "A Simplified Method for Culture of Endothelial-Cells and Analysis of Adhesion of Blood-Cells under Conditions of Flow." Microvascular Research **45**(1): 33-45.
- Cooke B. M., W. M., Coppel R. L. (2000). "Falciparum Malaria: Sticking Up, Standing Out, and Out-Standing." Parasitology Today **16**(10): 416-420.
- Cooke B.M. and Coppel R.L. (1995). "Cytoadhesion and Falciparum Malaria: Going with the flow." Parasitology Today **11**(8): 282-287.
- Gascoyne P., Mahidol C., Ruchirawat M., Satayavivad J., Watcharasit P. and Becker F.F. (2002). "Microsample preparation by delectrophoresis: isolation of malaria." Lab on a Chip **2**(2): 70-75.
- Groves, J. T. (1996). Notes on Electrostatics at a Dielectric-Solution Interface.
- Gruenberg J., A. D. R., Sherman I. W. (1983). "Scanning electron microscope-analysis of the protrusions (knobs) present on the surface of *Plasmodium falciparum*-infected erythrocytes." The Journal of Cell Biology **97**: 795-802.
- Hycr, K., A. Wilczek and K. Cieszka (1993). "Electrophoretic Heterogeneity of Pigmented Hamster Melanoma-Cells." Pigment Cell Research **6**(2): 100-110.
- Ichiki T., Ujiie T., Shinbashi S., Okuda T. and H. Y. (2002). "Immunoelectrophoresis of red blood cells performed in microcapillary chips." Electrophoresis(23): 2029-2034.
- Kakkilaya, B. S. (2006, April 29, 2006). "Malaria Site: Comprehensive Malaria Website."
- Mehrishi J. N. and Bauer J. (2002). "Electrophoresis of cells and the biological relevance of surface charge." (23): 1984-1994.
- Methal N. Albarghouthi, T. M. S. A. E. B. (2003). "Poly-N-hydroxyethylacrylamide as a novel, adsorbed coating for protein separation by capillary electrophoresis." ELECTROPHORESIS **24**(7-8): 1166-1175.
- Minerick A. R., Ostafin A. E. and C. H-C. (2002). "Electrokinetic transport of red blood cells in microcapillaries." Electrophoresis(23): 2165-2173.
- Nagao E., K. O., Dvorak J. A. (2000). "*Plasmodium Falciparum*-Infected Erythrocytes: Qualitative and quantitative analyses of parasite-induced knobs by atomic force microscopy." Journal of Structural Biology **130**: 34-44.
- Nash G. B., Cooke B. M., Marsh K., Berendt A., Newbold C. and S. J. (1992). "Rheological analysis of the adhesive interaction of red blood cells parasitized by *Plasmodium Falciparum*." Blood **79**(3): 798-807.

- Omasu F., Nakano Y. and Ichiki T. (2005). "Measurement of the electrophoretic mobility of sheep erythrocytes using microcapillary chips." Electrophoresis **26**: 1163-1167.
- Sabolovic D., Sestier C., Perrotin P., Guillet R., Tefit M. and Boynard M. (2000). "Covalent binding of polyethylene glycol to the surface of red blood cells as detected and followed up by cell electrophoresis and rheological methods." Electrophoresis **21**: 301-306.
- Schasfoort R. B. M., Schlautmann S., Hendrikse J. and van den Berg A. (1999). "Field-Effect Flow Control for Microfabricated Fluidic Networks." Science **286**(29): 942-945.
- Shelby P.J., White J., Ganesan K., Rathod P.K. and C. D.T. (2003). "A microfluidic model for single-cell capillary obstruction by *Plasmodium Falciparum*-infected erythrocytes." PNAS **100**(25): 14618-14622.
- Slivinsky G. G., Hymer W. C., Bauer J. and Morrison D. R. (1997). "Cellular electrophoretic mobility data: A first approach to a database." Electrophoresis **18**(7): 1109-1119.
- Sutton N., Tracey M. C., Johnston I. D., Greenway R. S. and Rampling M. W. (1997). "A novel instrument for studying the flow behaviour of erythrocytes through microchannels simulating human blood capillaries." Microvascular Research **53**: 272-281.
- Thomas Burg, A. B. (2006). Communications regarding pressure driven flow of erythrocytes in microchannels. K. Naegle. Boston.
- WHO (2006). Malaria in Africa. [www.rbm.who.int](http://www.rbm.who.int), World Health Organization.

## Table of Figures

Figure 1: Comparison of a healthy red blood cell, a red blood cell in trophozoite stage, and a red blood cell in schizont stage (from left to right). Protrusions density increases with stage of infection. SEM images taken from (Gruenberg J. 1983). .....	8
Figure 2: a) Cross-section of proposed microfluidic FET device (not drawn to scale). Controllable wall charge of device allows for optimal interaction between device walls and cell wall of parasitically infected RBC. b) Picture of proposed microcapillary device, whose walls are functionalized with a receptor protein. Interactions between the cell membrane proteins and the wall receptors result in a velocity decrease of diseased cells. . .	11
Figure 3: Interactions occurring between a PRBC and an endothelial cell resulting from parasite encoded adhesion proteins (Cooke, 2000). .....	14
Figure 4: (Shelby P.J., White J. et al. 2003) Microcapillary constrictions 2 $\mu$ m high, with varying widths shows that later stages of PRBC cannot pass through channel widths smaller than 6 $\mu$ m. Arrow indicate direction of pressure driven flow. ....	18
Figure 5: Cross section of proposed device (not drawn to scale). Initial channel height, 2 $\mu$ m. Device widths ranging from 2-20 $\mu$ m. ....	19
Figure 6: Microscope pictures of fabricated devices a) 8 $\mu$ m snake-like channel and bypass on left b) Glass bypass and silicon through-hole interconnect.....	21
Figure 7: Depiction of dielectric-solution interface with metal electrode gate. The double layer, consisting of the compact Stern layer (Cs) and the diffusion layer (Cd) are in series with the dielectric capacitance (Cd).....	22
Figure 8: Surface Potential vs. applied voltage as a function of intrinsic surface potential (which is dependent on solution pH). ....	25
Figure 9: Zeta potential as a function of voltage for various ionic concentrations, and therefore debye lengths, with a neutral intrinsic wall charge.....	26
Figure 10: Surface potential vs. voltage for varying ionic concentrations where intrinsic wall potential is -100mV.....	27
Figure 11: (Omasu F., Nakano Y. et al. 2005) Comparison of different wall coatings and their effect on electroosmotic flow.....	28
Figure 12: Oxide breakdown voltage and gate voltage as function of oxide thickness. Gate voltage solved to achieve 100mV zeta potential with a -50mV intrinsic potential at 1mM ionic strength.....	30
Figure 13: Fluid velocity ( $\mu$ m/s) vs. applied gate voltage for a 50V/cm lateral electric field, zero intrinsic wall charge, and a 100mM ionic strength solution.....	33
Figure 14: Picture of straight 4 $\mu$ m channel. Boxes above and below channel designed to aid in image recognition.....	35

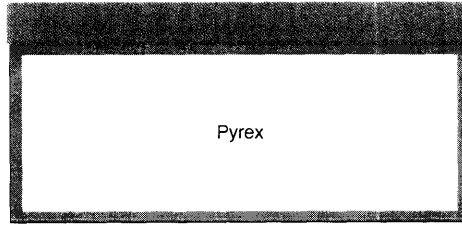
## Table of Equations

Equation 1: Gouy Equation	$\zeta_o(\sigma) = \left(\frac{2kT}{ze}\right) \sinh^{-1}\left(\frac{\sigma ze L_D}{2kT\epsilon}\right)$	..... 23
Equation 2: Debye length	$L_D \equiv \left(\frac{kT\epsilon}{2Iz^2e^2}\right)^{\frac{1}{2}}$	..... 23
Equation 3: Gouy Capacitance of the diffuse layer	$C_G = \frac{\epsilon}{L_D} \cosh\left(\frac{ze\zeta}{2kT}\right)$	..... 23
Equation 4: Capacitance due to the silicon oxide dielectric	$C_D = \frac{\epsilon_{ox}}{t_{ox}}$	..... 23
Equation 5: Capacitor divider	$dV = \frac{C_G}{C_D} d\zeta$	..... 24
Equation 6: Zeta potential with applied gate bias	$\zeta(V) = \frac{2kT}{ze} \sinh^{-1}\left[\left(\frac{zeL_D C_D}{2kT\epsilon}\right)V + \sinh\left(\frac{ze\zeta_o}{2kT}\right)\right]$	..... 24
Equation 7: Voltage required to achieve a desired zeta potential	$V = \left(\frac{2kT\epsilon}{zeL_D C_D}\right) \left[\sinh\left(\frac{ze\zeta}{2kT}\right) - \sinh\left(\frac{ze\zeta_o}{2kT}\right)\right]$	..... 29
Equation 8: Fluid velocity resulting from electroosmosis	$v_f = \frac{\epsilon}{\eta} \zeta E$	..... 33
Equation 9: Fluid velocity as a function of applied gate voltage V	$v_f = \frac{2kT}{ze} \sinh^{-1}\left[\left(\frac{zeL_D C_D}{2kT\epsilon}\right)V\right] \frac{\epsilon}{\eta} E$	..... 33
Equation 10: Average fluid velocity for one-dimensional laminar flow	$v_f = \frac{h^2}{2\eta} \frac{\Delta P}{\Delta x}$	..... 36
Equation 11: Induced electric field due to streaming potential	$E = \frac{\Delta V}{\Delta x} = \frac{h^2}{2\epsilon} \frac{1}{\zeta} \frac{\Delta P}{\Delta x}$	..... 36
Equation 12: Smoluchowski equation, with Huckel's correction, relating zeta potential and EPM	$EPM = \frac{U}{Eo} = \frac{2}{3} \frac{\epsilon\zeta}{\eta}$	..... 38
Equation 13: EPM as a function of surface charge density	$EPM = \frac{2}{3} \frac{\sigma}{L_d \eta}$	..... 38

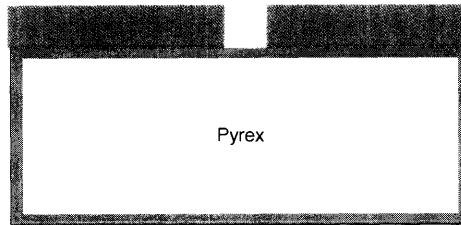
# Appendix – Process Flow

## Pyrex Processing

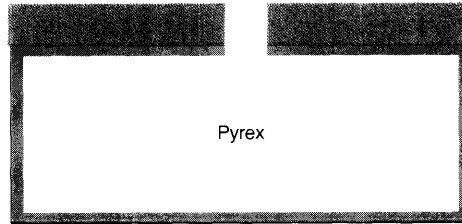
Spin Coat Positive photoresist



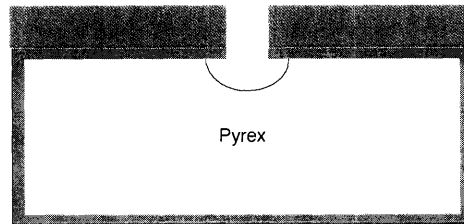
Pattern Resist



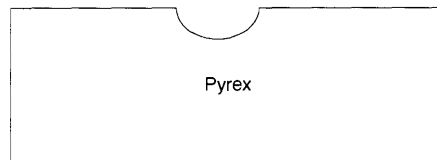
Etch alpha-Si mask  
RIE



Etch Glass Channels  
49% HF



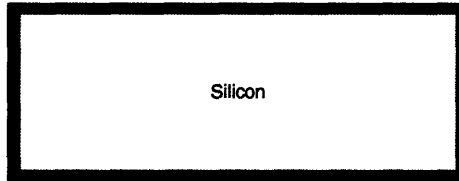
Strip Resist – pirhana  
Strip Silicon mask - HNA



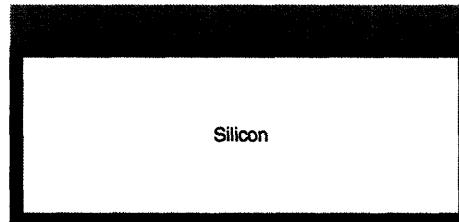


# Silicon Processing

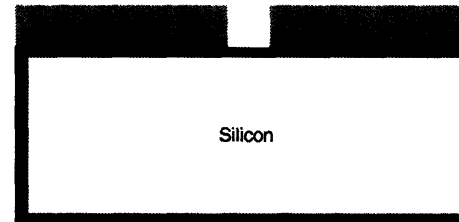
VTR Nitride growth



Spin Coat positive photoresist

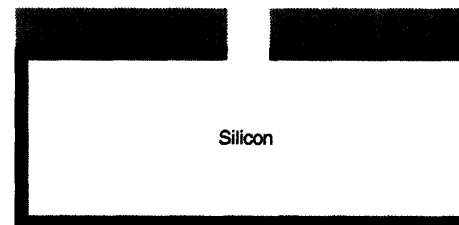


Pattern Resist



Etch nitride for through-holes  
RIE

Remove Resist



**KOH Etch Throughholes**  
**Post-KOH Clean**



**Spincoat and Pattern Backside Resist**

**Nitride etch channels RIE**  
**Silicon etch channels**  
**Remove Resist**

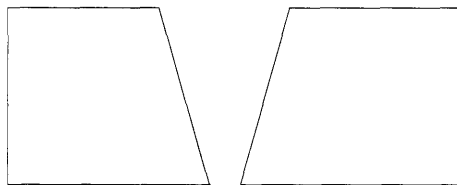
**Post-KOH Clean**



**Remove nitride mask – hot phosphoric acid**



**RCA Clean**  
**Oxide growth (500nm)**



**Anodic Bonding**  
**300°C, 800V**

